

Surface-wave eikonal tomography for dense geophysical arrays

Pierre Gouédard¹, Huajian Yao^{1,2}, Fabian Ernst³, and Robert D. van der Hilst¹

¹*Earth, Atmospheric and Planetary Sciences department, Massachusetts Institute of Technology,*

²*Institute of Geophysics and Planetary Physics, Scripps Institution of Oceanography,*

³*Shell Projects and Technology*

SUMMARY

Surface-wave tomography often involves the construction of phase (or group) velocity maps through linearized inversion of measured phase (group) arrival times. Such inversions require *a priori* information about the medium (that is, a reference model) in order to calculate source-receiver paths, which is inaccurate for complex media, and requires regularization. The surface-wave eikonal tomography proposed here bypasses these limitations and has the advantage of being simple to implement and use, with virtually no input parameters. It relies on accurate phase arrival time measurement, which can be challenging for dispersive waves and complex waveforms. We present a measurement method based on the evaluation of phase arrival time differences at nearby receivers. We show, using an exploration data set, that the produced Rayleigh-wave velocity maps are in agreement with results from traditional tomography, but the latter have lower resolution due to the need of regularization to accommodate for the heterogeneity of the study area and noise in data. Eikonal tomography requires averaging over results from multiple sources to produce a proper image, and we evaluate this requirement to a 200 m source spacing in the considered scattering environment. In addition, we validate the approach of combining seismic

interferometry and eikonal tomography, for the cases where the source coverage is inappropriate.

Key words: Tomography; Interferometry; Controlled source seismology; Seismic tomography; Surface waves and free oscillations

1 INTRODUCTION

Surface waves are of increasing interest in exploration geophysics, in particular for overburden characterization, as they provide information about shallow structures (*e.g.*, Campman & Riyanti 2007; Socco & Boiero 2008). They are usually processed using a local layered medium approximation to obtain, in a first step, phase- or group-velocity maps for specific frequencies, which in a second step are then inverted into a S- (and sometimes P-) wave velocity model at shallow depth (*e.g.*, Luo et al. 2008). The first step usually requires a ray tracer to compute traveltimes in the chosen model, which implies some underlying approximations about how waves propagate in the medium. We present here a different approach to surface-wave tomography: surface-wave eikonal tomography combined with a neighborhood-based cross-correlation method for phase arrival picking. This data driven approach takes advantage of the high density receiver arrays that are common in exploration seismics and can deal with complex media and waveforms. Eikonal tomography neither needs *a priori* information nor ray tracing (because it uses a local equation, the eikonal equation, to describe wave propagation) and has become possible for seismic exploration as recent technological advances made sub-wavelength spatial sampling feasible. It is easy to implement and produces results that are robust and not dependent on the choice of input parameters. Eikonal tomography has been successfully applied in a global seismology context, using ambient noise wavefields, to image crustal structure beneath western North America using the EarthScope/USArray Transportable Array (Lin et al. 2009).

Measuring the phase arrival times that are used as input for this type of velocity analysis is challenging when working with waveforms that are complex owing to dispersion and scattering. Lin et al. (2009) built traveltime maps from (virtual) source–receiver phase measurements in narrow frequency bands. Direct measurement is efficient if the medium varies smoothly on a spatial scale that is (much) larger than the wavelengths of the waves considered, but is not accurate in the presence of scattering and multi-pathing. To improve the quality of traveltimes measurements when dealing with complex waveforms, we propose a traveltime

picking algorithm that is based on the integration of delays between neighboring receivers (obtained from cross-correlation).

In the first section of this paper we present the theory of eikonal tomography and the phase measurement algorithm that we use. In a second part we apply surface-wave eikonal tomography to data from a hydrocarbon exploration experiment for velocity analysis of a strongly heterogeneous and scattering medium. In a third section we use this data set for source depopulation—that is, we quantify the source spacing that is necessary to obtain a reliable velocity model for the area. The final section is devoted to the validation of the combination of seismic interferometry and eikonal tomography, which is useful when the coverage of active sources is not suitable for traditional eikonal tomography.

2 THEORY AND METHODS

2.1 Eikonal tomography

Traveltime tomography concerns the estimation of spatial variations in the propagation speed of seismic waves from a set of traveltimes of seismic phases between known source and receiver locations. Essentially, the traveltime is an integration (averaging) of the local wave slowness over the source–receiver paths:

$$t(\mathbf{r}_s, \mathbf{r}_r) = \int \frac{K(\mathbf{r}, \mathbf{r}_s, \mathbf{r}_r)}{c(\mathbf{r})} d\mathbf{r} \quad , \quad (1)$$

where t is the traveltime from a source in position \mathbf{r}_s to a receiver in position \mathbf{r}_r , $c(\mathbf{r})$ is the local structural phase velocity that we want to recover, and K is the integration kernel. The integration is done over 3-D space, but the spatial extent of the wave sensitivity depends on the theoretical approximations made: in the case of ray theory K vanishes everywhere except along the ray, whereas it is oscillatory (with non-zero values away from the ray) in the case of finite frequency wave theory (Dahlen et al. 2000; de Hoop & van der Hilst 2005). Traveltimes measurements are classically inverted, in a “de-integration” operation, to map local phase velocity in the sampled area.

A different approach would be to use

$$|\nabla t(\mathbf{r}_s, \mathbf{r})|^2 = \frac{1}{c_s^2(\mathbf{r})} + \frac{\Delta A}{A\omega^2} \quad , \quad (2)$$

which is derived from the Helmholtz equation (*e.g.*, Wielandt 1993; Friederich et al. 2000). In (2), $\Delta = \nabla^2$ is the Laplacian, ω the angular frequency, and A the amplitude of the waves. The latter includes source and receiver site effects and propagation effects (attenuation, scattering, interferences. . .). When using this equation to infer the local wavespeed, the inversion process

(if any) takes place when building the traveltime map, and not in a “de-integration” step as in classical traveltime tomography. Notice that for surface waves equation (2) is an approximation as these waves do not, in general, obey the Helmholtz equation. It is valid, however, if we neglect mode conversions and the directivity of scattering from a point heterogeneity, which is justified as long as the medium can be considered locally homogeneous, *i.e.*, if it is only slightly or smoothly inhomogeneous compared to the heterogeneity of the wavefield (Friederich et al. 1993). The Helmholtz equation can be used for laterally heterogeneous media if the receiver network is dense enough to account for the interferences among several plane waves and the second spatial derivatives of the wavefield be accurately estimated (Friederich et al. 2000). Lin et al. (2011) applied this technique, which they called Helmholtz tomography, to earthquake surface-wave data to image the crust beneath the western part of the contiguous United States.

The second term on the right-hand side of equation (2) accounts for finite frequency effects and can sometimes be neglected, which leads to the eikonal equation:

$$|\nabla t(\mathbf{r}_s, \mathbf{r})|^2 \approx \frac{1}{\hat{c}^2(\mathbf{r})} \quad . \quad (3)$$

Strictly speaking, \hat{c} is the dynamic velocity, which is affected by propagation effects (and in particular by the curvature of the wavefront and interference with other waves) and not the structural velocity c used in (2), which represents the medium properties (Wielandt 1993; Friederich et al. 2000). While true only for plane waves, we assume here that \hat{c} equals c . Lin et al. (2009) used his equation to image the lithosphere of Western USA from ambient seismic noise.

In principle, the traveltime t (in equations (2) and (3)) needs to be known at each point of the study area, but the gradient can be computed with sufficient accuracy if t is measured at receivers on a dense grid (which is usually the case in seismic exploration). Any source and receiver geometry is suitable for this method, provided that the sensor spacing is sufficiently dense and realizing that interpolation may be needed to fill gaps in the spatial sampling or to map the recording points on a regular grid to ease the computation of the numerical gradient.

Equation (3) can be used to construct phase velocity maps for specific frequencies. In our study we use it to produce phase velocity maps of the Rayleigh-wave fundamental mode. In a second step, the dispersion curves at each location of the map could then be inverted for a local (shear-wave) velocity profile as function of depth (Park et al. 1999; Socco & Strobbia 2004), and lateral juxtaposition of these depth profiles would then form (with interpolation, if necessary) 3-D volumes of shear wavespeed. This second step requires *a priori* information about the medium and is not done here.

The above procedure is straightforward and easy to implement, but we make a few comments. First, we note that the point-wise inversion for local shear wavespeed profiles (that is, the second step) renders the mapping between data and structure essentially asymptotic. Second, consideration of azimuthal anisotropy is straightforward, as shown by Lin et al. (2009). Indeed, the vectorial form of equation (3) gives directly access to the wave-vector $\mathbf{k}_s(\mathbf{r}) = (\omega/\hat{c}_s(\mathbf{r})) \mathbf{u}_s(\mathbf{r})$, where $\mathbf{u}_s(\mathbf{r})$ is the local propagation direction at point \mathbf{r} for a source at \mathbf{r}_s , and $c_s(\mathbf{r})$ is the local velocity at this point and for this direction. Keeping track of both the norm and the direction of \mathbf{k}_s (\mathbf{u}_s being different for each source position) allows getting velocity-versus-azimuth plots at each pixel of the final map, which usually gives the information about azimuthal anisotropy. Because of limitations of the data set, however, we did not consider this possibility in this paper. Third, there is no limitation to use eikonal tomography either for other surface-wave modes (including Love waves if two horizontal components of the wavefield are available) or for body waves (provided that t can be measured on a 3-D grid, which is not usually practical).

2.2 Phase arrival time measurements

Taking the gradient is a numerically unstable operation and measuring the phase arrival times must be done with great care to ensure a smooth traveltimes map. The dispersive nature of the surface waves used in this study makes it difficult to define the arrival time. Moreover, scattering can produce complex waveforms (as is the case in our study) making it difficult to track individual phases. To address these observational challenges we propose a neighborhood-based cross-correlation method to measure arrival time differences between nearby receivers. This method is similar to the multi-channel cross-correlation method (Vandecar & Crosson 1990), in which each trace is cross-correlated with all other traces to obtain the relative time shifts, but we limit the correlation to nearby stations in order to avoid cycle-skipping and ensure similar waveforms. For each source s , the relationship between the arrival time differences between receivers and the source–receiver traveltimes can be written

$$\mathbf{D} \mathbf{t}^s = \Delta \mathbf{t}^s \quad , \quad (4)$$

where \mathbf{D} is a differentiation matrix (a sparse matrix with one ‘+1’ and one ‘-1’ per line) of size $N_r \times N_r(N_r - 1)/2$ (N_r being the number of receivers), $\mathbf{t}^s = (t_i^s)_{i=1\dots N_r}$ is the vector of traveltimes at each receiver, and $\Delta \mathbf{t}^s = (\Delta t_{ij}^s = t_j^s - t_i^s)_{i=1\dots N_r, j=1\dots N_r}$ is the vector of measured arrival time differences between receivers, from cross-correlation of narrow-band filtered (fundamental mode) surface waves. The number of pairs of receivers considered in

practice may vary, depending on data quality and medium heterogeneity, but we will limit ourselves to the closest neighbors. The measurement error on $\Delta\mathbf{t}^s$ is evaluated as the width of the 90 % confidence interval from the correlation of waveforms.

Equation (4) describes a Bayesian problem, which can be solved with a quasi-Newton method (*e.g.*, Tarantola 2005):

$$\mathbf{t}^s \approx \tilde{\mathbf{D}}^{-1} \Delta\mathbf{t}^s \quad , \quad (5)$$

where $\tilde{\mathbf{D}}^{-1}$ is the pseudo-inverse of the differentiation matrix \mathbf{D} (that is, $\tilde{\mathbf{D}}^{-1}$ is an integration matrix), which can be written as

$$\tilde{\mathbf{D}}^{-1} = \left(\mathbf{D}^T \mathbf{C}_D^{-1} \mathbf{D} + \mathbf{C}_M^{-1} \right)^{-1} \mathbf{D}^T \mathbf{C}_D^{-1} \quad , \quad (6)$$

where \mathbf{D}^T denotes the transpose of \mathbf{D} , \mathbf{C}_D is a data covariance matrix, and \mathbf{C}_M is a model covariance matrix. For \mathbf{C}_D we use a diagonal matrix with elements are proportional to the measurement error in $\Delta\mathbf{t}$. Regularization is introduced by choosing a second order differentiation matrix for \mathbf{C}_M^{-1} . This definition of the covariance matrix ensures a traveltimes map close to the one expected for an homogeneous model (the second derivative of the traveltimes with respect to the distance is null).

As $\tilde{\mathbf{D}}^{-1}$ is an integration operator, \mathbf{t}^s is defined modulo a constant of integration. This ambiguity could be resolved by extrapolating the traveltimes \mathbf{t}^s towards zero offset, where it has to be zero, but this is difficult in practice because traveltimes measurements at short offsets from the source (within one or two wavelengths) are not reliable due to near field effects (figure 2b). The value of the integration constant is irrelevant, however, because we are only interested in the gradient of \mathbf{t}^s (see equation (2)).

Equations (3) and (5) may suggest that our approach is equivalent to double difference tomography (Zhang & Thurber 2003). It is different, however, because we do not have to include any *a priori* information, such as a starting model and we do not have to trace any rays because the ray information is naturally included in the gradient from equation (2). For a more complete discussion on how rays are handled in eikonal tomography we refer to Lin et al. (2009).

3 APPLICATION FOR SHALLOW SUBSURFACE IMAGING

3.1 Data and pre-processing

For our study we use data from a high-resolution survey of a 1 km \times 1 km carbonate (karst) area in Northern Oman conducted by Petroleum Development Oman (PDO). Receiver points

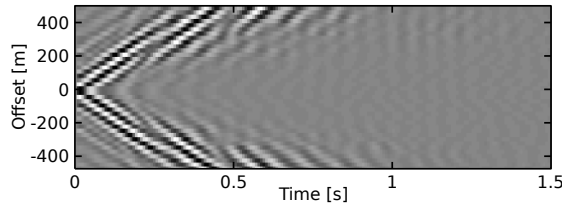


Figure 1. A shot gather, band-pass filtered between 10 and 20 Hz, illustrating the complexity of the waveform. The amplitude is normalized.

are located at the nodes of a 40×40 grid (25 m \times 25 m spacing). Each receiver point consists of a cluster of 12 vertical geophones, from which data are stacked on-site. Sources are vibrator trucks acting at the nodes of a similar grid, shifted with respect to the receiver grid by half a grid distance in both directions (that is, 12.5 m). Records are 4 s long and the sampling frequency is 125 Hz. For a more complete description of the data set, we refer to Herman & Perkins (2006) and Gouédard et al. (2008). Figure 1 illustrates the complexity of the waveforms produced by scattering.

The complete data set consists of 1600×1600 vertical component source–receiver time-domain signals, and constitutes an exhaustive measurement of the transfer functions of the half-space medium over a 1-km² area. Because of the 2-D acquisition geometry the data set includes mainly Rayleigh waves.

Records are first filtered around the different working frequencies using a Gaussian filter of 10 % width. The central frequencies considered in the following are 10 Hz, 15 Hz and 20 Hz. The filtered waveforms are then windowed in time around the maximum of the envelope, corresponding to the fundamental mode Rayleigh wave in this small scale setup.

3.2 Inversion and discussion

To account for possible data quality reduction due to noise when using real data we subjected the measured traveltimes differences Δt to quality control. The correlation-based approach that we used to measure Δt assumes that the recorded waveforms are similar between neighbors. We thus used the correlation coefficient between these waveforms, windowed around the fundamental mode Rayleigh wave, as a quality criterion. We choose a threshold value of 0.98 for this correlation coefficient, and any measurement with smaller value is not considered. This procedure typically rejects 30 % of the measurements for each source. This data selection helps stabilize the inversion for a single source, but when results from different sources are stacked this selection is not critical because the implied averaging smooths out the outliers in single-source velocity models. For instance, lowering the threshold value to 0.9 would result

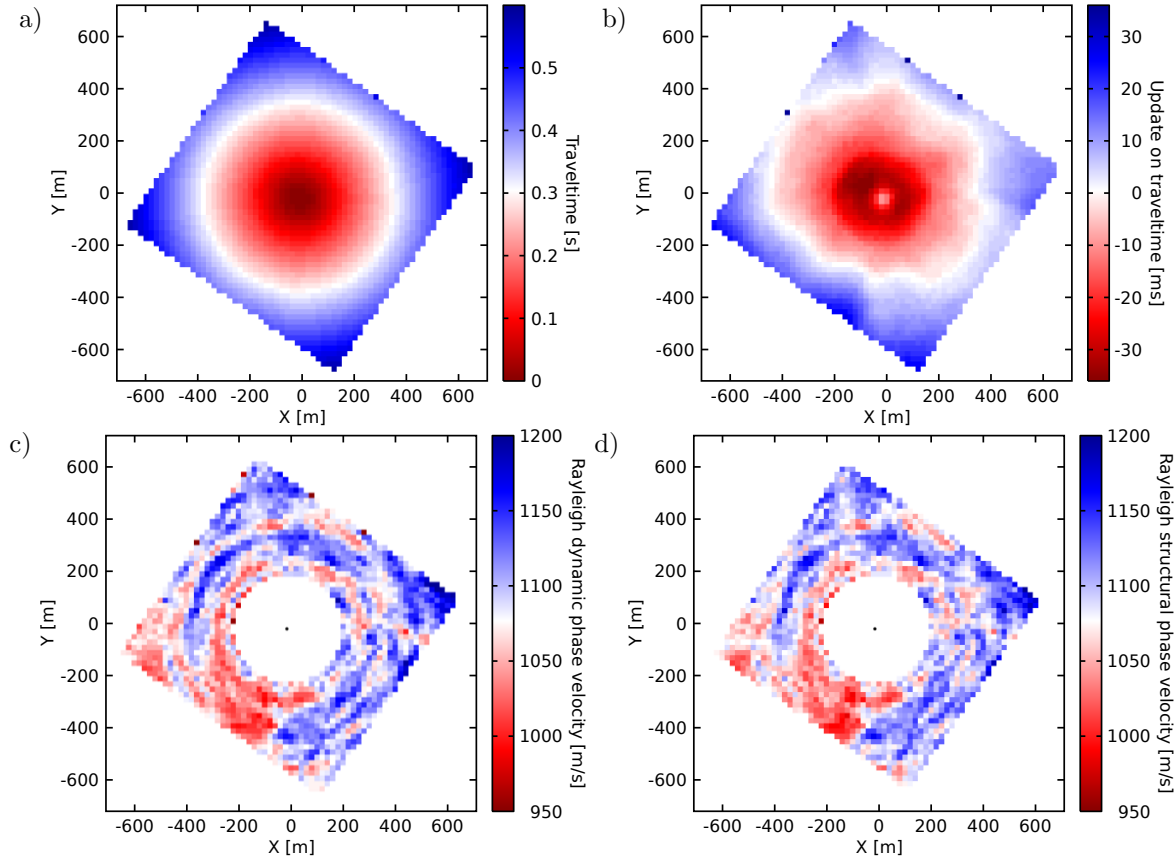


Figure 2. **a.** Traveltime map for the fundamental mode Rayleigh wave at 15 Hz, for one source located at the center of the array. **b.** Same as **a.**, but with the mean gradient (1187 m/s) removed to emphasize differences with an homogeneous medium (for illustration purposes only, not used in the inversion). **c.** Dynamic phase velocity map for this source, obtained from the spatial gradient of the map in **a.**, following equation (3). The source location is indicated by the black dot in the center of the array. Offsets smaller than 200 m are omitted because of their unreliability due to near field effects (Lin et al. 2009). **d.** Structural phase velocity map for this source, obtained following equation (2).

in the rejection of less than 0.5 % of the measurements but produces a final velocity map that differs by less than 0.5 % (on a per-pixel basis) from the one presented on figure 4a.

Equation (2) (or (3)) can be used to produce maps of the structural (or dynamic) velocity from a single source (figure 2). Subsequently, phase velocity maps from all sources can be combined, which leads to the velocity maps presented in figures 3a and 3b for average dynamic and structural velocities, respectively.

Structural velocity is preferred, as it represents a medium property, but the calculation of the dynamic velocity is easier and numerically more stable because it avoids the calculation of the second derivative and division by the amplitude. Moreover, equation (2) is not easy to use because the recorded Rayleigh wave amplitudes are not always meaningful or accurate. In

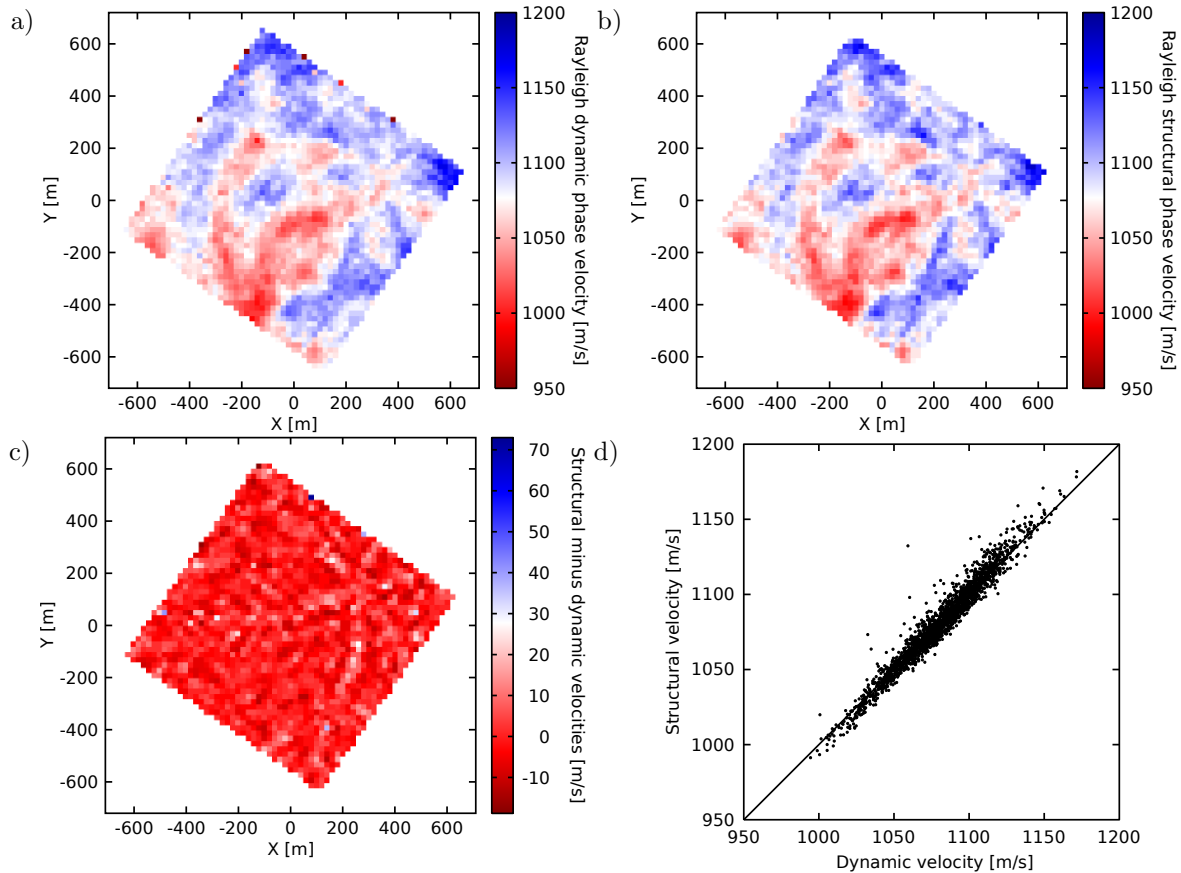


Figure 3. Comparison of the Rayleigh wave fundamental mode **a.** dynamic and **b.** structural phase velocity maps, at 15 Hz. **c.** Difference of the two maps (structural minus dynamic). **d.** Cross-plot of the dynamic and structural velocities for each pixel.

our data set, for instance, the records are not from a single receiver but from a cluster of 12 receivers so that the original amplitudes are not retained. Figures 2 and 3 demonstrate that the differences between the two velocities are small and do not have any spatial structure, which justifies the use of the dynamic velocity (which avoids the above-mentioned issues with amplitude).

Figure 3a presents the Rayleigh-wave phase velocity at 15 Hz and results for two other frequencies are presented in figures 4a and 4b. These maps reveal strong medium heterogeneity. This heterogeneity would complicate any tomography that requires ray tracing, such as traditional or double-difference tomography, and it is likely that in such applications much of the structural details inferred here would have been lost due to regularization. We note that the averaged slowness values at each frequency match values found by Gouédard et al. (2011, figure 2) for a laterally-homogeneous equivalent medium for this area. The observed increase of velocity with increasing frequency may be a bias due to scattering (Kaelin & Johnson

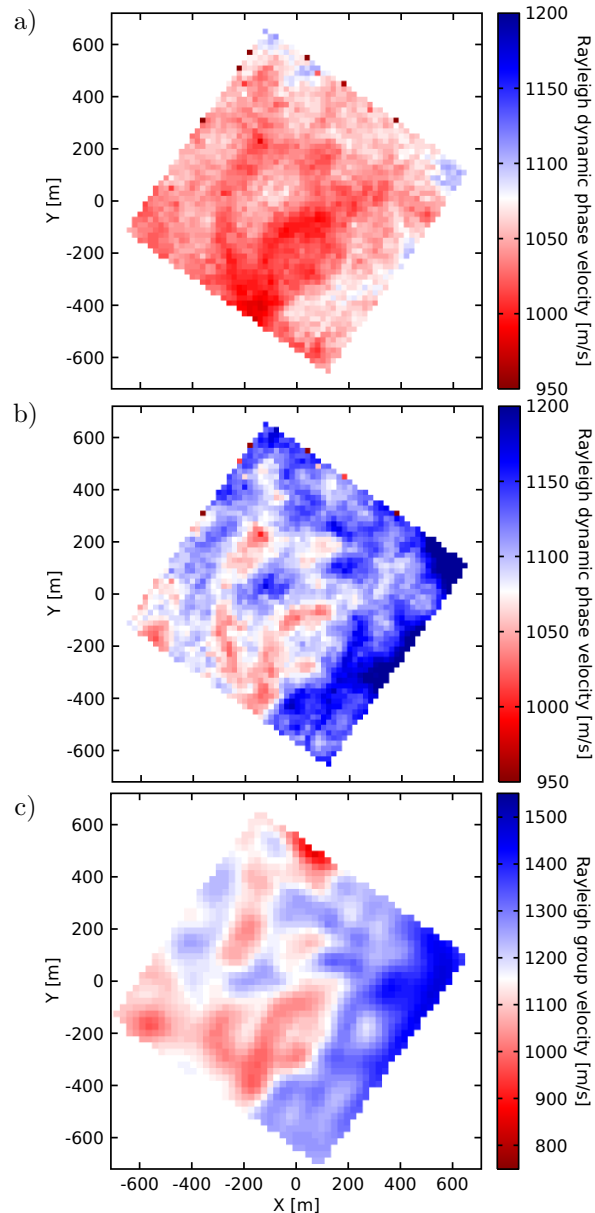


Figure 4. Rayleigh-wave phase-velocity maps obtained from eikonal tomography at **a.** 10 Hz; and **b.** 20 Hz. **c.** Rayleigh-wave fundamental mode group velocity obtained using traveltimes tomography (from Gouédard et al. (2011))

1998), or it could represent a real depth variation in average wavespeed—and, hence, material properties—with depth.

We recall that a 3-D velocity model can be obtained from velocity maps such as presented in figure 4 (but then calculated for a range of frequencies) through point-wise inversion of the (fundamental mode Rayleigh-wave) dispersion curve for a S- and P-wave velocity profile with depth (*e.g.*, Socco & Strobbia 2004; Luo et al. 2008). This requires *a priori* information

# of sources	400	100	25	9	1
R	0.9995	0.9926	0.9612	0.8542	0.7285

Table 1. Correlation coefficients R between the Rayleigh-wave phase velocity maps obtained by decreasing the number of sources, and the map obtained using the 1600 available sources.

about the medium (in order to calculate the proper sensitivities to relate dispersion to elastic medium properties at different depths) and is not done here.

In figure 4c we show the group velocity model obtained by Gouédard et al. (2011) from the same data. Gouédard et al. (2011) used a traveltimes tomography approach to produce a fundamental mode Rayleigh-wave group velocity map (as opposed to phase velocity here) in a broader frequency band (10–25 Hz) than considered here. Despite the differences in inversion method, frequency content, and wave type, the results are consistent: while the tomography result is smoother due to regularization and the use of lower frequency data, the main structures of figures 3a, 4a and 4b are also present in figure 4c. We also checked (not shown here) that approximating the group slowness with the frequency derivative of the phase slowness times the frequency yields a map close to the one displayed in figure 4c. This comparison shows that, as expected, eikonal tomography yields higher resolution maps.

3.3 Source depopulation: How many sources are necessary?

The averaging over multiple sources suppresses the effects of wave propagation (due to medium heterogeneity) on the estimation of dynamic velocity from equation (3) (Friederich 1998). A question that immediately arises is how many sources are actually necessary to recover a good velocity model. To address this question, we conducted a source depopulation exercise by considering fewer and fewer sources in the averaging process, as illustrated by figure 5. Notice that figure 2c completes the series, with only one source, located at the center of the image area. To assess the quality of model reconstruction we compare the obtained velocity models to the one obtained using all available sources (figure 4b), which we assume to be the best possible recovery of the medium fundamental mode Rayleigh wave velocity. The comparison is done by computing the correlation coefficient R between the value of the velocity at each pixel. Table 1 shows that using 25 sources instead of the 1600 available (200 m spacing instead of 25 m) degrades the result only slightly. An *a posteriori* comparison of figures 4b and 2c also shows that, despite having more artifacts, the map obtained with only one source already includes the main features of the final map.

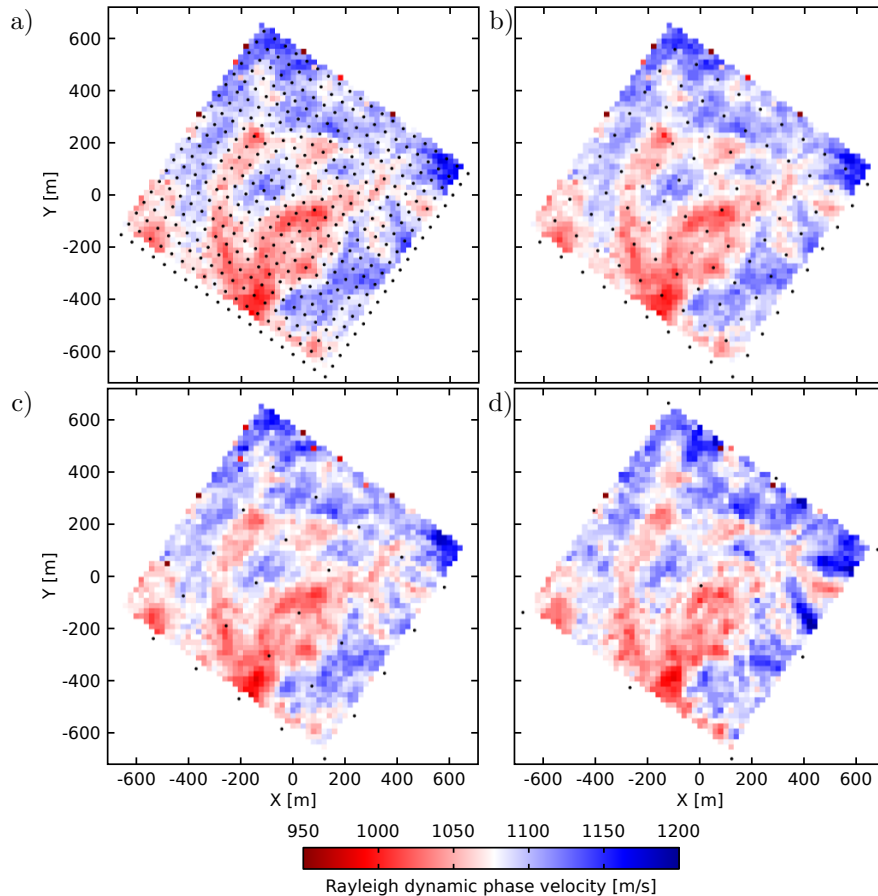


Figure 5. Source depopulation at 15 Hz. Maps are obtained by using less sources than the 1600 available involved to produce figure 4b. The number of sources (which locations are indicated by the black dots) used for each figure is as follow: **a.** 400 sources (one over two in both directions); **b.** 100 sources (one over four in both directions); **c.** 25 sources; **d.** 9 sources. Figure 2c completes the series with only one source used.

4 INTERFEROMETRY

We discussed above how averaging over sources helps to get a reliable velocity model. Another practical limitation comes from the source distribution, *i.e.*, the actual location of these sources. Even though, in theory, any source/receiver geometry is suitable for the technique to work (as long as the receiver array is sufficiently dense), in practice only a limited range of source–receiver offsets can be used. Traveltime measurements in the near field are not reliable, as illustrated by figure 2, which defines the short offset limit. At offsets that are too large, poor signal-to-noise ratio prevents the traveltime differences between neighbors to be measured accurately. These practical limits can obstruct the construction of velocity maps for the whole array.

It is well established that (under appropriate conditions) cross-correlation of a wavefield recorded at two receivers can yield the Green’s function for waves propagating between them, (*e.g.*, Campman et al. 2005; Gouédard et al. 2008, 2011, for applications in a prospecting context). This technique, usually referred-to as seismic interferometry, allows one to have a virtual source at any of the receiver locations. In the context of this paper it allows the transformation of the source–receiver geometry constraints to receiver–receiver constraints, which are easier to satisfy thanks to the dense receiver array.

The interferometric workflow is similar to the one presented above, but preceded by the Green’s function reconstruction. This step consists in considering pairs of receivers and averaging the cross-correlation of records at each receiver over a distribution of sources. Following the discussion in Gouédard et al. (2008), we chose to consider sources in the alignment of the receiver pair (the so-called endfire lobes). This ensures a good reconstruction of direct waves, even if only a few sources are recorded by the two receivers, and also avoids inappropriate azimuthal energy distribution in the wavefield. The cross-correlation functions are then symmetrized by stacking their positive- and negative-time sides. The reconstructed Green’s functions are used as an input to eikonal tomography, as if a source was located at one of the receivers. The resulting maps, at the same frequencies as used before, are presented in figure 6. These maps are comparable to these from figure 4, which demonstrates the feasibility of interferometric eikonal tomography, using active source, similar to using seismic ambient noise (Lin et al. 2009).

We note that interferometric reconstruction of the amplitude of the Green’s functions is still a topic of research and is not guaranteed in a general setup and processing workflow (Gouédard et al. 2008; Cupillard & Capdeville 2010; Lin et al. 2011), only dynamic velocities can be obtained using this approach.

5 CONCLUSIONS

We propose an alternative approach to imaging subsurface from surface waves, namely surface-wave eikonal tomography (combined with a neighborhood-based cross-correlation method for traveltimes measurement), which overcomes some important limitations of traveltimes tomography, *viz* the need of *a priori* information about medium heterogeneity and loss of short-wavelength structure due to regularization. Our approach takes advantage of the high density of receiver arrays, which allows the use of a local equation to link traveltimes and phase velocity (instead of the integral relationship used for traveltimes tomography), is easy to implement and use, and does not require *a priori* information (*e.g.*, a starting model).

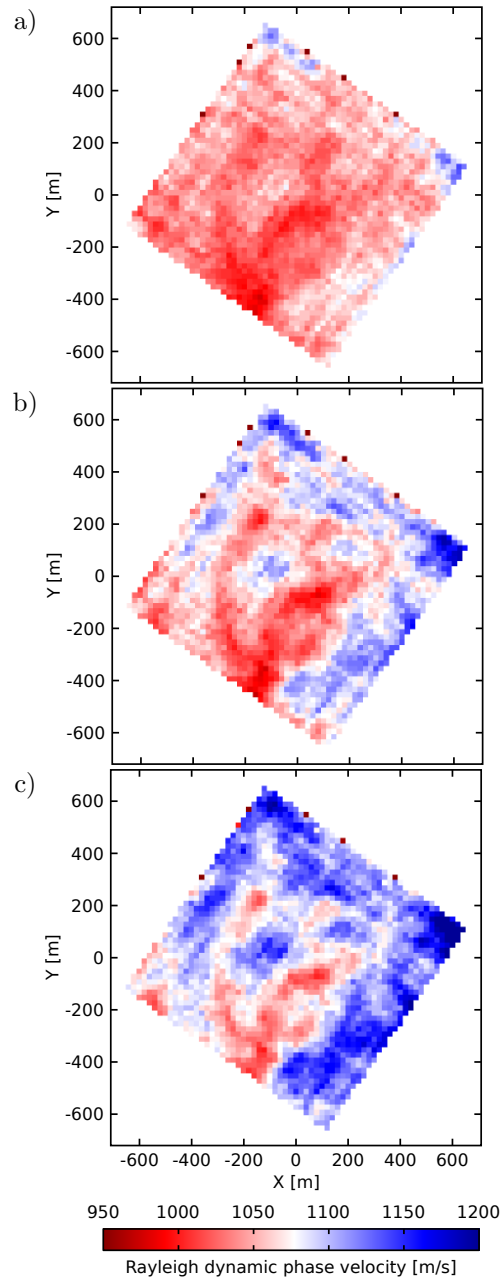


Figure 6. Same as figures 3a and 4a–b, but from eikonal tomography applied to reconstructed Green’s functions obtained with seismic interferometry. As a reminder, the considered frequency bands are: **a.** 10 Hz; **b.** 15 Hz; and **c.** 20 Hz.

We showed that, at least in the wavenumber ranges used in this study, dynamic phase velocity can effectively replace structural phase velocity, making the inversion numerically more stable and the results more robust since amplitude information is not always accurately preserved during pre-processing.

Surface-wave eikonal tomography requires a dense receiver array as well as numerous

sources. We studied the effect of reducing the number of sources, in a source-depopulation exercise, and showed that (for the medium used in our study) a 200 m source spacing is sufficient to produce an adequate image. When source coverage is not appropriate, either in terms of spatial distribution or number of sources, seismic interferometry can produce virtual records that can be used as input for eikonal tomography.

6 ACKNOWLEDGMENTS

The authors thank the Ministry of Oil and Gas of the Sultanate of Oman, Petroleum Development of Oman and Shell Research for permission to use the data and publish these results. The authors are also grateful to Arie Verdel, formerly at Shell International Exploration & Production B. V., and now at Delft University of Technology, for his help in starting this project, and for the stimulating discussions that followed. PG is supported by a Shell Research grant.

REFERENCES

- Campman, X. & Riyanti, C. D., 2007. Non-linear inversion of scattered seismic surface waves, *Geophysical Journal International*, **171**(3), 1118–1125.
- Campman, X. H., van Wijk, K., Scales, J. A., & Herman, G. C., 2005. Imaging and suppressing near-receivers scattered surface waves, *Geophysics*, **70**(2), V21–V29.
- Cupillard, P. & Capdeville, Y., 2010. On the amplitude of surface waves obtained by noise correlation and the capability to recover the attenuation: a numerical approach, *Geophysical Journal International*, **181**(3), 1687–1700.
- Dahlen, F. A., Hung, S.-H., & Nolet, G., 2000. Fréchet kernels for finite-frequency traveltimes—I. Theory, *Geophysical Journal International*, **141**(1), 157–174.
- de Hoop, M. V. & van der Hilst, R. D., 2005. On sensitivity kernels for ‘wave-equation’ transmission tomography, *Geophysical Journal International*, **160**(2), 621–633.
- Friederich, W., 1998. Wave-theoretical inversion of teleseismic surface waves in a regional network: phase-velocity maps and a three-dimensional upper-mantle shear-wave-velocity model for southern Germany, *Geophysical Journal International*, **132**(1), 203–225.
- Friederich, W., Wielandt, E., & Stange, S., 1993. Multiple forward scattering of surface waves: Comparison with an exact solution and Born single-scattering methods, *Geophysical Journal International*, **112**(2), 264–275.
- Friederich, W., Hunzinger, S., & Wielandt, E., 2000. A note on the interpretation of seismic surface waves over three-dimensional structures, *Geophysical Journal International*, **143**(2), 335–339.
- Gouédard, P., Roux, P., Campillo, M., & Verdel, A., 2008. Convergence of the two-point correlation

function toward the Green's function in the context of a seismic prospecting data set, *Geophysics*, **73**(6), V47–V53.

Gouédard, P., Roux, P., Campillo, M., Verdel, A., Yao, H., & van der Hilst, R. D., 2011. Source depopulation potential and surface wave tomography using a crosscorrelation method in a scattering medium, *Geophysics*, **76**(2), SA51–SA61.

Herman, G. C. & Perkins, C., 2006. Predictive removal of scattered noise, *Geophysics*, **71**(2), V41–V49.

Kaelin, B. & Johnson, L., 1998. Dynamic composite elastic medium theory. Part II. Three-dimensional media, *Journal of Applied Physics*, **84**(10), 5458–5468.

Lin, F.-C., Ritzwoller, M. H., & Snieder, R., 2009. Eikonal tomography: surface wave tomography by phase front tracking across a regional broad-band seismic array, *Geophysical Journal International*, **177**(3), 1091–1110.

Lin, F.-C., Ritzwoller, M. H., & Shen, W., 2011. On the reliability of attenuation measurements from ambient noise cross-correlations, *Geophysical Research Letters*, **38**, L11303.

Luo, Y., Xia, J., Liu, J., Xu, Y., & Liu, Q., 2008. Generation of a pseudo-2D shear-wave velocity section by inversion of a series of 1D dispersion curves, *Journal of Applied Geophysics*, **64**(3-4), 1115–1124.

Park, C. B., Miller, R. D., & Xia, J., 1999. Multichannel analysis of surface waves, *Geophysics*, **64**(3), 800–808.

Socco, L. V. & Boiero, D., 2008. Improved Monte Carlo inversion of surface wave data, *Geophysical Prospecting*, **56**(3), 357–371.

Socco, L. V. & Strobbia, C., 2004. Surface-wave method for near-surface characterization: a tutorial, *Near Surface Geophysics*, **2**(4), 165–185.

Tarantola, A., 2005. *Inverse problem theory and methods for model parameter estimation*, Society for Industrial and Applied Mathematics.

Vandecar, J. C. & Crosson, R. S., 1990. Determination of teleseismic relative phase arrival times using multi-channel cross-correlation and least squares, *Bulletin of the Seismological Society of America*, **80**(1), 150–169.

Wielandt, E., 1993. Propagation and structural interpretation of non-plane waves, *Geophysical Journal International*, **113**(1), 45–53.

Zhang, H. & Thurber, C. H., 2003. Double-difference tomography: The method and its application to the Hayward Fault, California, *Bulletin of the Seismological Society of America*, **93**(5), 1875–1889.